



HAL
open science

Fan-shaped jet close to a light bridge

Y. Liu, G. P. Ruan, B. Schmieder, S. Masson, Y. Chen, J. T. Su, B. Wang, X.
Y. Bai, Y. Su, W. Cao

► **To cite this version:**

Y. Liu, G. P. Ruan, B. Schmieder, S. Masson, Y. Chen, et al.. Fan-shaped jet close to a light bridge. Astronomy and Astrophysics - A&A, 2022, 667, 10.1051/0004-6361/202243292 . insu-03874875

HAL Id: insu-03874875

<https://insu.hal.science/insu-03874875>

Submitted on 28 Nov 2022

HAL is a multi-disciplinary open access archive for the deposit and dissemination of scientific research documents, whether they are published or not. The documents may come from teaching and research institutions in France or abroad, or from public or private research centers.

L'archive ouverte pluridisciplinaire **HAL**, est destinée au dépôt et à la diffusion de documents scientifiques de niveau recherche, publiés ou non, émanant des établissements d'enseignement et de recherche français ou étrangers, des laboratoires publics ou privés.



Distributed under a Creative Commons Attribution 4.0 International License

Fan-shaped jet close to a light bridge[★]

Y. Liu¹, G. P. Ruan¹, B. Schmieder^{2,3,4}, S. Masson⁵, Y. Chen¹, J. T. Su⁶, B. Wang¹, X. Y. Bai⁶,
Y. Su^{7,8}, and W. Cao^{9,10}

¹ Shandong Provincial Key Laboratory of Optical Astronomy and Solar-Terrestrial Environment, and Institute of Space Sciences, Shandong University, Weihai 264209, PR China

e-mail: rgp@sdu.edu.cn

² Observatoire de Paris, LESIA, Université PSL, CNRS, Sorbonne Université, Université de Paris, 5 place Jules Janssen, 92190 Meudon, France

³ University of Glasgow, School of Physics and Astronomy, Glasgow G128QQ, Scotland, UK

⁴ Centre for Mathematical Plasma Astrophysics, Dept. of Mathematics, KU Leuven, 3001 Leuven, Belgium

⁵ Laboratoire de Physique des Plasmas (LPP), Ecole Polytechnique, IP Paris, Sorbonne Université, CNRS, Observatoire de Paris, Université PSL, Université Paris-Saclay, Paris, France

⁶ Key Laboratory of Solar Activity, National Astronomical Observatories, Chinese Academy of Sciences, Beijing 100012, PR China

⁷ Key Laboratory of Dark Matter and Space Astronomy, Purple Mountain Observatory, Chinese Academy of Sciences (CAS), 8 Yuanhua Road, Nanjing 210034, PR China

⁸ School of Astronomy and Space Science, University of Science and Technology of China, Hefei, Anhui 230026, PR China

⁹ Center for Solar-Terrestrial Research, New Jersey Institute of Technology, 323 Martin Luther King Blvd., Newark, NJ 07102, USA

¹⁰ Big Bear Solar Observatory, New Jersey Institute of Technology, 40386 North Shore Lane, Big Bear City, CA 92314-9672, USA

Received 9 February 2022 / Accepted 2 May 2022

ABSTRACT

Aims. On the Sun, jets in light bridges (LBs) are frequently observed with high-resolution instruments. The respective roles played by convection and the magnetic field in triggering such jets are not yet clear.

Methods. We report a small fan-shaped jet along a LB observed by the 1.6m Goode Solar Telescope (GST) with the TiO Broadband Filter Imager (BFI), the Visible Imaging Spectrometer (VIS) in H_{α} , and the Near-InfraRed Imaging Spectropolarimeter (NIRIS), along with the Stokes parameters. The high spatial and temporal resolution of those instruments allowed us to analyze the features identified during the jet event. By constructing the H_{α} Dopplergrams, we found that the plasma is first moving upward, whereas during the second phase of the jet, the plasma is flowing back. Working with time slice diagrams, we investigated the propagation-projected speed of the fan and its bright base.

Results. The fan-shaped jet developed within a few minutes, with diverging beams. At its base, a bright point was slipping along the LB and ultimately invaded the umbra of the sunspot. The H_{α} profiles of the bright points enhanced the intensity in the wings, similarly to the case of Ellerman bombs. Co-temporally, the extreme ultraviolet (EUV) brightenings developed at the front of the dark material jet and moved at the same speed as the fan, leading us to propose that the fan-shaped jet material compressed and heated the ambient plasma at its extremities in the corona.

Conclusions. Our multi-wavelength analysis indicates that the fan-shaped jet could result from magnetic reconnection across the highly diverging field low in the chromosphere, leading to an apparent slipping motion of the jet material along the LB. However, we did not find any opposite magnetic polarity at the jet base, as would typically be expected in such a configuration. We therefore discuss other plausible physical mechanisms, based on waves and convection, that may have triggered the event.

Key words. Sun: activity – sunspots – Sun: atmosphere – Sun: photosphere – Sun: chromosphere – Sun: corona

1. Introduction

Solar jets are collimated ejections of plasma in the solar atmosphere. They are a means of mass and energy transport through the heliosphere and, thus, it is important to understand their formation mechanisms. They commonly consist of multi-thermal components of cool and hot plasma, respectively referred to as surges and X-ray jets (see reviews in [Raouafi et al. 2016](#); [Shen 2021](#); [De Pontieu et al. 2021](#); [Schmieder et al. 2021](#)).

The cool plasma of surges ($<10^4$ K) related to light bridges (LBs) was first investigated in the 1970s by [Roy \(1973\)](#). In a detailed study of four surges combining H_{α} observations with

vector magnetograms, these authors computed the velocity and the length of the surges and obtained a maximum value for the speed around 175 km s^{-1} and a maximum length of 50 Mm. After an ascending phase, a descending phase was observed with an acceleration smaller than the gravity. Later, LBs were studied by [Asai et al. \(2001\)](#) using the Transition Region and Coronal Explorer (TRACE), demonstrating smaller ejections (23 Mm length) with a fan-shape as with the jets examined by [Roy \(1973\)](#).

The size of such jets spans broad range domains, from 200 Mm at the edge of active regions to small scale of 1–2 Mm that is related to network and sunspot penumbra. The kinetic energy of jets is related to speed from 10 km s^{-1} to 300 km s^{-1} . Large jets seen in the chromosphere are often long-lasting and

* Movie associated to Fig. 1 is available at <https://www.aanda.org>

recurring. They have other signatures, such as brightenings at their footpoint in the chromosphere, as well as hot jets in the transition region and corona. Their associated hot jets are observed in different wavelengths, from the extreme ultraviolet to the X-ray (Joshi et al. 2020). Over the past decade, thanks to the high spatial and temporal resolution observations in optical range by advanced telescopes such as the Solar Optical Telescope (SOT, Tsuneta et al. 2008) on board the Hinode spacecraft, the Interface Region Imaging Spectrograph (IRIS, De Pontieu et al. 2014), the New Vacuum Solar Telescope (NVST, Liu et al. 2014), the Swedish Solar telescope (SST, Scharmer & Lofdahl 1991), and the Goode Solar Telescope (GST, Goode & Cao 2012), smaller and smaller jets have been detected (e.g., Shibata et al. 2007; Katsukawa et al. 2007; Tian et al. 2014; Peter et al. 2014; Louis et al. 2008; Iijima & Yokoyama 2017; Yang et al. 2019a; Ruan et al. 2019; Li et al. 2020).

With the development of these instruments, intense research has been carried out on active ejections. The chromosphere above sunspots exhibits many various dynamic phenomena such as running penumbra waves, umbra flashes, vortex flows, and jets – particularly in cases when the spot has a fragmented penumbra or a LB (e.g; Louis et al. 2008; Yang et al. 2019a; Asai et al. 2001; Robustini et al. 2016, 2018; Li et al. 2020; Lim et al. 2020). It is known that LBs have a weaker magnetic field compared to the surrounding umbra, with the magnetic field lines more inclined over the solar surface than in the umbra (Toriumi et al. 2015a,b). With the SOT on board of Hinode, small jets were observed by the wide-band pass Ca II filter (e.g., Shimizu et al. 2009; Louis et al. 2014). Shimizu et al. (2009) reported on a sunspot LB that produced chromospheric plasma ejections intermittently and recurrently for more than one day. It has been explained that EUV jets and H_α surges represent hot and cool plasma ejections, respectively, along different field lines because they are not co-spatial at high spatial resolution (Chae et al. 1999). The jets above LB may reach up to the lower corona and the front is heated up to transition region and coronal temperatures (Bharti 2015; Yuan & Walsh 2016). Long spicules (sometimes referred to as small jets) are observed in H_α and may provide hot plasma to the corona and most of the enhanced spicules are thought to channel hot plasma into the corona (Samanta et al. 2019).

The magnetic configuration of LBs shows frequently opposite magnetic polarities compared to the surrounding umbra (Toriumi et al. 2015b; Bharti et al. 2007; Lim et al. 2020). Therefore the most well known model of jet formation is energy release by magnetic reconnection in the chromosphere (Heyvaerts et al. 1977; Shibata et al. 2007; Chae et al. 1999; Shimizu et al. 2009). Tian et al. (2018), Lim et al. (2020) found opposite magnetic polarities at the light bridge, opening the possibility of a reconnection between the emerging flux and the surrounding sunspot field. But the trigger of the acceleration is not well understood. The cool material can be accelerated by magnetic tension of reconnected field lines and create a slingshot effect (Nishizuka et al. 2008), or by slow shock waves colliding with the transition region (Shibata 1982; Takasao et al. 2013). In fact, Shibata (1982) distinguished two types of macrospicules depending on the density of the shock regions: shocks in the transition region or shock waves originate in network bright points in the photosphere, with the latter potentially creating shock-tube type jets.

Opposite polarities are sometimes difficult to evidence in LBs. Bai et al. (2019) studied a fan-shaped jet caused by convective motions in the photosphere and could detect parasitic polar-

ity at the jet base after applying a special treatment to the Stokes parameter profiles as well as Franz & Schlichenmaier (2013). In these cases, the authors found abnormal Stokes V profiles revealing a configuration of three lobes. The detection of a third lobe in the Stokes V profiles demonstrates the presence of opposite polarity. The detection of three-lobe profiles in their analysis induced an increase of the area of opposite polarity in the penumbra from 4% to 17%.

Another possible way of triggering jets is from the MHD waves from the photosphere, whereby shocks could be formed from magneto-acoustic waves caused by the leakage of p -mode oscillations or by Alfvén waves that push the plasma inside the flux tubes by increasing the pressure in magnetic concentration like in macrospicules (Shibata 1982). In recent simulations, chromospheric jets were produced by shock waves passing through the transition region. Iijima & Yokoyama (2015) found that the scale of chromospheric jets is related to the temperature of the ambient corona. By using two-dimensional (2D) magnetohydrodynamic simulations, they found that shorter jets exist in relatively cooler corona, as in coronal holes. Various excited MHD waves could produce chromospheric jets in three-dimensional (3D) simulations (Iijima & Yokoyama 2017). The results show that the simulated jets are closely related to solar spicules. Later on, it was shown that numerical simulations concerning the Sun compared to laboratory fluid dynamics experiments could explain the formation mechanism of the jets. Under the effects of gravity, the non-linear focusing of quasi-periodic waves in an anisotropic media of both magnetized plasma and polymer fluid is sufficient to generate a large number of jets similar to chromospheric spicules (Dey et al. 2022). This MHD wave domain should be investigated further in future to explore the initiation of jets.

At the base of surges, brightenings in chromospheric lines have been observed. Studies have found that the footpoint brightening of plasma ejection from a LB is similar to Ellerman bombs (Bharti et al. 2007). Their line profiles have been compared with Ellerman bombs (EBs) or IRIS bombs (IBs) (Yang et al. 2019b; Joshi et al. 2021). An EB has enhanced emission in the H_α wings and commonly no signature in H_α line core (Ellerman 1917; Rezaei & Beck 2015; Grubecka et al. 2016; Chen et al. 2019). It is thought to be triggered by magnetic reconnection in the lower atmosphere from 50 to 900 km above the solar surface (Grubecka et al. 2016). On the other hand, brightenings in the umbra, called umbra dots have been explained by convection bringing above the solar surface hotter plasma and could be responsible for the LB formation (Katsukawa et al. 2007). LBs in a sunspot favor the decay of the spot and its submergence by convective flows. This idea has been also investigated in the sunspot formation simulation of Rempel (2012), where it was shown that hot bubbles from the convection may invade umbra and penumbra, serving as tools for fragmenting sunspots.

There are several major debates centered around the formation of tiny jets in sunspot LB, particularly regarding the role played by magneto-convection and by magnetic reconnection.

In this paper, we present high-resolution observations of a fan-shaped jet obtained by the Goode Solar Telescope (GST) operating at the Big Bear Solar Observatory (BBSO), as well as by the Atmospheric Imaging Assembly (AIA) aboard the Solar Dynamic Observatory (SDO). We consider the dynamic evolution of the jet flow and the vector magnetograms in Sect. 2. In Sect. 3, we summarize our results and discuss the implications of our observations on explaining the trigger mechanisms of LB jets.

2. Observations

2.1. Instruments

On August 25, 2016, a fan-shaped jet was observed in the leading sunspot of the NOAA active region AR 12579 located at N11W22¹ with the Big Bear Solar Observatory (BBSO) coupled with the 1.6 meter Goode Solar Telescope (GST) (Goode & Cao 2012) as well as the Solar Dynamic Observatory (SDO) (Pesnell et al. 2012) coupled with the Atmospheric Imaging Assembly (AIA) (Lemen et al. 2012). The pointer of the GST was centered on the leading spot of the active region. We focused the field of view on the LB in a small field of view around 17'' × 17''.

The GST data contain simultaneous observations of the photosphere, using the titanium oxide (TiO) line taken with the Broadband Filter Imager, and the chromosphere, using the H_α 6563 Å line obtained with the Visible Imaging Spectrometer (VIS; Cao et al. 2010). The passband of the TiO filter is 10 Å, centred at 705.7 nm, while its temporal resolution is about 15 s with a pixel scale of 0''.034. Concerning the VIS, a combination of 5 Å interference filter and a Fabry-Pérot etalon is used to get a bandpass of 0.07 Å in the H_α line. The VIS field of view (FOV) is about 70'' with a pixel scale of 0''.029. To obtain more spectral information, we scan the H_α line at 11 positions with a 0.2 Å step following this sequence: ±1.0, ±0.8, ±0.6, ±0.4, ±0.2, 0.0 Å. We obtained a full Stokes spectroscopic polarimetry using the Fe I 1565 nm doublet over a 85'' round FOV with the aid of a dual Fabry-Pérot etalon by the NIRIS Spectropolarimeter (Cao et al. 2012). Stokes I , Q , U , and V profiles were obtained every 72 s with a pixel scale of 0''.081. All TiO and H_α data were speckle reconstructed using the Kiepenheuer-Institute Speckle Interferometry Package (Wöger et al. 2008).

We analyze the EUV multi-wavelength imaging data from SDO/AIA, the vector magnetic field, and continuum intensity data by the Helioseismic and Magnetic Imager (HMI) (Schou et al. 2012) on board the SDO spacecraft. AIA observes the Sun in ten different wavebands, covering a wide range of temperatures and reveals physical processes at various layers of the solar atmosphere. The pixel size of the data is 0''.6 and the temporal cadence is 12 s. Generally, HMI provides four main types of data: dopplergrams (maps of solar surface velocity), continuum filtergrams (broad-wavelength photographs of the solar photosphere), and both line-of-sight and vector magnetograms (maps of the photospheric magnetic field). The processed HMI continuum intensities and magnetograms data are obtained with a 45 s cadence and a 0''.6 pixel size, provided by the HMI team. Here, we mainly used the data from seven EUV channels of AIA and HMI continuum intensity. For comparison with NIRIS we analyzed the HMI magnetograms in the 24 h before the event. Continuum intensity maps of HMI help us to co-align the TiO, H_α images and the magnetograms taken by GST. The GST images taken at each wavelength position were internally aligned using the cross-correlation technique provided by the BBSO programmers. The co-alignment between SDO/HMI continuum and GST images was achieved by comparing commonly observed features of sunspots in Fe I 6173 Å images and TiO, H_α ± 0.8 Å images taken frame by frame.

2.2. Fan-shaped jet

In the present work, we are interested in a fan-shaped jet invading the umbra of the leading negative sunspot of AR 12579 observed in the H_α lines with the GST. The event occurs between 18:42:43 UT and 19:16:00 UT. Figure 1 shows the temporal evolution of the event for three wavelengths: TiO, H_α − 0.8 Å and H_α + 0.8 Å at four different times.

The dark structure of the fan-shaped jet that was initially identified was observed at 18:52:46 UT. Its footpoint is located in the sunspot at $[x, y] = [313'', 97'']$ and the fan's extremities are located between $[x, y] = [313.8'', 94.6'']$ and $[x, y] = [314.8'', 94.9'']$ in the H_α blue wing at −0.8 Å (Fig. 1, panel b1). During this first phase, between 18:52:46 UT and 19:00:23 UT, the fan's beams display a sweeping motion from the south toward the north (Fig. 1, left column). The extension of each beam of the jet is around 2.5 arcsec, close to 2000 km, and the width of each beam is about 21 km. Prior to this jet appearing, there were other mini jets but lasting only for 4–5 min, so we do not analyze them here.

We computed the height-time diagram of the fan-shaped jet northward edge to determine its projected propagation speed. It first propagates at 3.15 km s^{−1} until ≈18:57 UT and then it accelerates to reach 6.91 km s^{−1} until 19:00 UT (Fig. 2, top-right panel). At 18:59:55 UT the fan extends from $[x, y] = [316'', 94.8'']$ to $[x, y] = [316.1'', 97.6'']$. At this time, we can also identify the fan-shaped jet in the H_α red wing at +0.8 Å.

A few seconds later, at 19:00:23 UT, the fan-shaped jet disappears in the H_α blue wing at −0.8 Å but it remains visible in the H_α red wing at +0.8 Å. Between 19:00:23 UT and 19:03:45 UT the dark material forming the fan-shaped jet seems to flow back down into the sunspot toward the footpoint. While in the first phase, the size of the fan increases with time, in the second phase, the fan's extension decreases with time.

2.3. Dopplergram of the fan-shaped jet

In order to determine the line-of-sight (LoS) velocity of the fan-shaped jet material, we created Doppler diagrams of the plasma using the H_α 11 wavelength images from the GST observations. We calculated the center of weight of the H_α line profile at each pixel to estimate the Doppler shift relative to the reference line center. We averaged the entire observing FOV to obtain the reference line center (except the region where the sunspot is located) and all the line profiles were corrected by comparing them with a standard H_α profile, obtained from the NSO/Kitt Peak FTS data (Su et al. 2016).

Dopplershift maps presenting the LoS velocities are shown in Fig. 3 with blue and red colors for the blue and redshift motions. Before 19:00:21 UT, the Doppler blueshift of the jet is dominant indicating plasma flowing upward, after that time the redshift is leading, indicating downward flows. According to the calculation of LoS velocities, we found that the upflow speed is up to −14.1 km s^{−1} and the downflow speed of the order of 9.5 km s^{−1}. Plasma fell back toward the chromosphere and four minutes later, the jet burst was complete.

2.4. Footpoint of the jet

At 18:52:54 UT, a small bright point is identified in the H_α red wing at +0.8 Å at the jet footpoint $[x, y] = [312.9'', 97'']$ highlighted by a red circle in Fig. 1, panel c1. Between 18:52:54 UT and 18:58:04 UT the intensity of this bright point increases and

¹ <https://www.solarmonitor.org/>

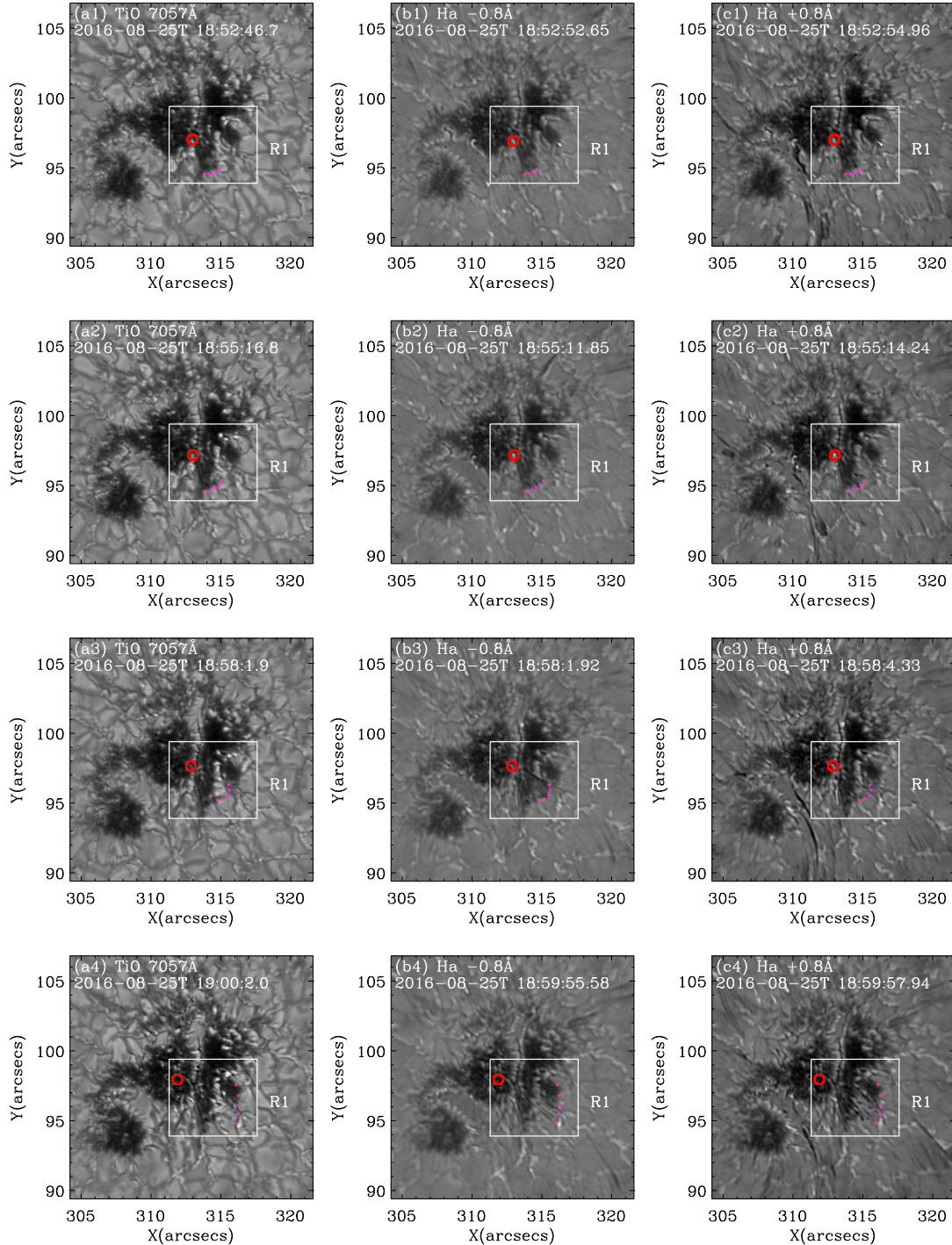


Fig. 1. Temporal evolution of a fan-shaped jet observed in the active region NOAA 12579 with the GST at BBSO on August 25 2016 between 18:52 UT and 18:59 UT. The different panels show: the TiO images (panels a1–a4), the H_{α} blue wing images at -0.8 \AA (panels b1–b4), and H_{α} red wing images at $+0.8 \text{ \AA}$ (panels c1–c4). All H_{α} images are obtained with the GST/VIS. R1 represents the area where the jet occurred (FOV of Figs. 2 and 4). The footpoint and front of the jet are marked by a red circle and magenta dots, respectively.

it moves northward up to $[x, y] = [312.8'', 97.6'']$ before totally disappearing at 18:58:04 UT. With a height-time diagram, we can determine the bright point velocity on the order of 2 km s^{-1} (Fig. 2, bottom-right panel).

We analyzed the characteristics of the H_{α} spectral lines at the jet footpoint. We normalized the intensity and exposure time of the H_{α} 11 wavelength images. The H_{α} profiles in the bright points corresponding to the jet footpoints are presented at three different times at 18:55:09, 18:55:57, 18:56:06 UT in

Fig. 4. They show a clear enhancement of intensity in the H_{α} line wings and no obvious signature in the H_{α} line core. These profiles are consistent with Ellerman bomb (EB) H_{α} line profiles (Pariat et al. 2007; Hashimoto et al. 2010; Watanabe et al. 2011; Rouppe van der Voort et al. 2016). It is worth noting that the reference H_{α} profile (averaged spectral profile of H_{α} on the quiet region) and the bright point profiles are symmetric. The intensity in the blue wing is very close to the one in the red wing which is typical of EB's profiles. Ellerman Bombs can be explained

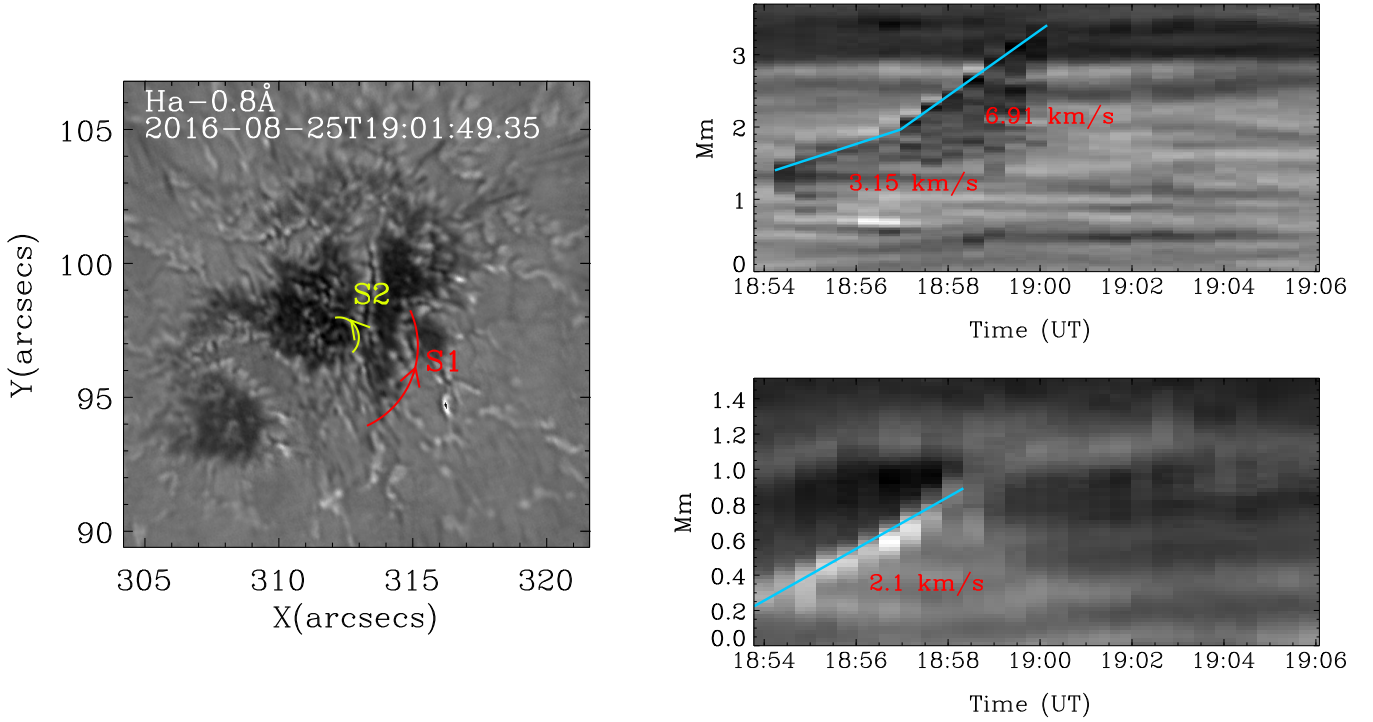


Fig. 2. Time slice diagrams in two slices marked in the $H\alpha$ blue wing image at -0.8 \AA (left panel). The right panels, from top to bottom, show the plasma trajectories moving along the S1 and S2 slices, respectively. S1 indicates the sweeping motion of the front of the jet and S2 the slipping motion of the bright footpoint of the jet, which ultimately invades the sunspot umbra. The footpoint of the jet moves by about 2.1 km s^{-1} which is around $12^\circ \text{ min}^{-1}$. The top of the jet moves with a speed of 6.9 km s^{-1} .

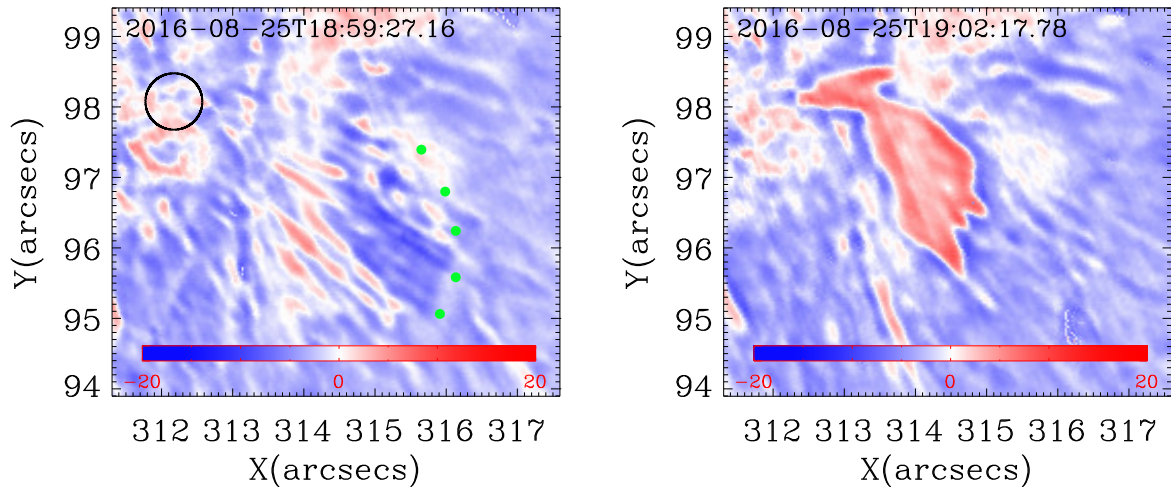


Fig. 3. LoS Doppler velocity maps obtained from GST/VIS of the zoom-in area of R1 (same field of view as in Fig. 4 bottom left). The footpoint and front of the jet are marked by a black circle and green dots, respectively.

as the radiative signatures of magnetic reconnection episodes occurring in the photosphere (Chen et al. 2001; Fang et al. 2006; Grubecka et al. 2016; Joshi et al. 2020). Therefore, observing EB's typical signature at the footpoints of the fan-shaped jet during the first phase, may indicate that the observed fan-shaped jet could have been driven by magnetic reconnection.

The active region is in a decaying phase with a very fragmented leading sunspot due to magneto-convection as it is shown in the TiO and $H\alpha$ wing images (see Fig. 1 and the corresponding movie). In the TiO and $H\alpha$ GST images (Fig. 1), the LB is clearly identified extending from $[x, y] = [311.3'', 95.8'']$ to $[x, y] = [313.8'', 101.2'']$. The bright point is moving along the LB axis. According to Tian et al. (2018), Lim et al. (2020), LBs

can be the signature of magnetic flux emergence inside a pre-existing sunspot. Therefore, magnetic reconnection may occur between the emerging flux and the sunspot magnetic field. The presence of a LB is an additional information supporting the fact that the bright point results from magnetic reconnection that could trigger the ejection of chromospheric material observed as the fan-shaped jet.

2.5. Photospheric magnetic field

Figure 5 left panel shows the NIRIS vector magnetogram of the sunspot at the time of 18:51:40 UT obtained by applying the Milne Eddington (ME) inversion to the Stokes profiles

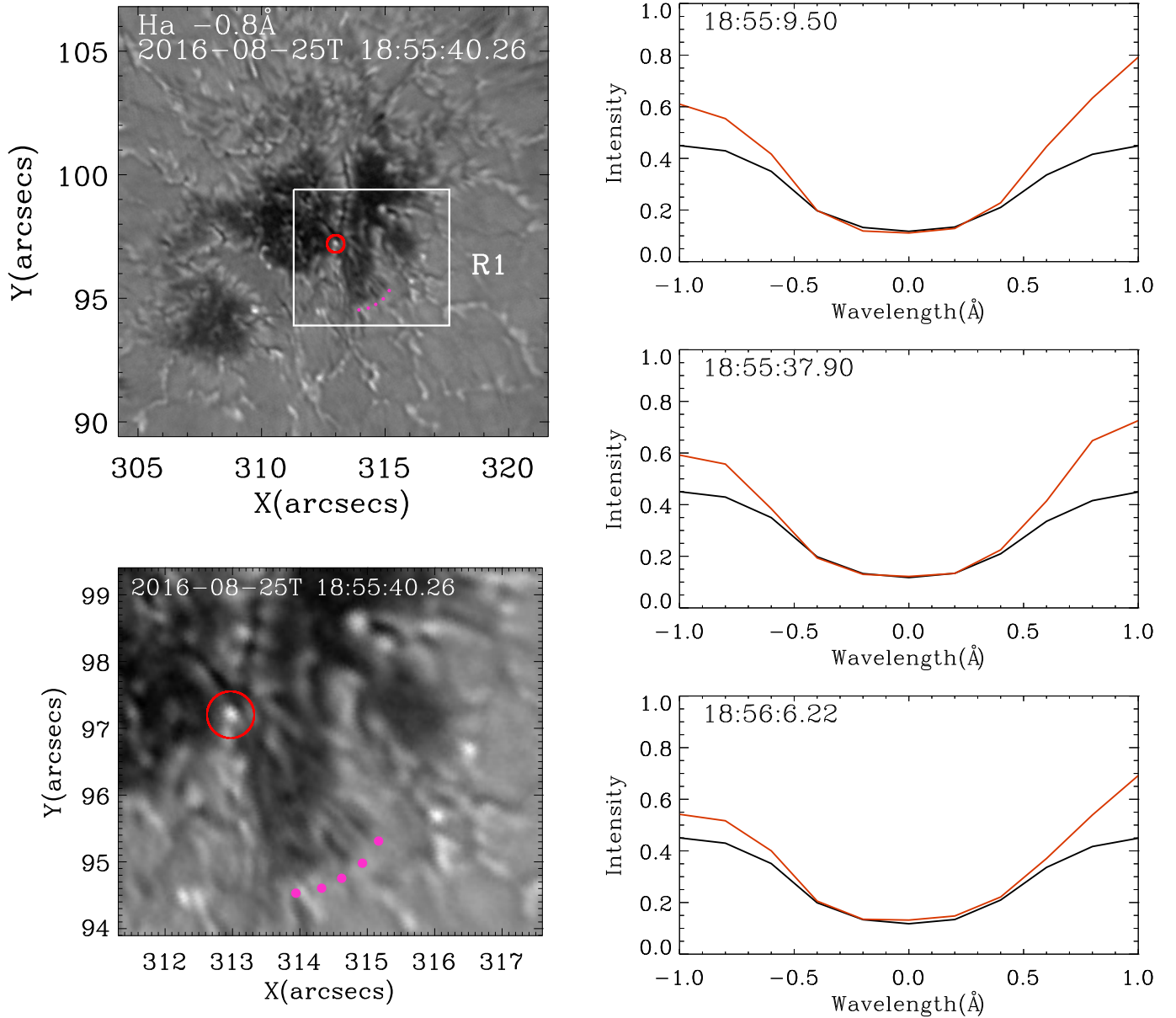


Fig. 4. Footpoint (red circle) and front of the jet (magenta dots) are marked in R1 region and in a zoom-in area of R1 (*left panels*). Normalized H_{α} spectral profile (red line) at the footpoint of the jet and reference profile (black line) for three times during magnetic reconnection are shown in the *right panels*.

of FeI 1565 nm doublet using the inversion code of J. Chae (Landi Degl’Innocenti 1992). The azimuth component of the inverted vector magnetic field was processed to remove the 180° ambiguity (Leka et al. 2009).

We find that the identified LB has a weaker vertical magnetic field (around 1000 Gauss) compared to the surrounding umbra (1700 Gauss) and the magnetic field in its upper part (from $[x, y] = [311.3'', 94'']$ to $[x, y] = [317.6'', 99.3'']$). The horizontal component of the magnetic field reaches also 1000 Gauss in the LB. The arrows in Fig. 5 (R1 box) indicate the direction of this component. They are highly inclined versus the axis of the LB close to the y axis with a tendency of being aligned with the main axis of the LB. This is in agreement with the description of the magnetic field in LBs (Leka 1997). However, we did not find a pure horizontal field (as would be expected for a LB) and we did not detect any opposite polarity in the area of the bright point which could lead to a jet-type reconnection as proposed in differ-

ent models of fan-shaped jet in LBs (Bharti 2015; Cheung et al. 2015; Robustini et al. 2018).

By computing the magnetic flux in the region R2, we found no emergence of new positive magnetic flux (see Fig. 6 on the flux in R2). Pixel by pixel, we analyzed the Stokes profiles to detect a third lobe but we could not identify such a pattern in the profiles, as done in the work by Bai et al. (2019). The difference of resolution of NIRIS compared to VIS is only a factor 2.8 and this cannot explain the non-visibility of an opposite polarity either.

The right panel in Fig. 5 displays a zoom on the R2 box of the left panel. It shows the south part of the LB where the bright point associated with the fan-shaped jet footpoint moves during the event. We observe a change in direction versus the x axis of the horizontal component evolving from a south-west to north-eastward orientation to a west-eastward orientation in the northern part. This change in the horizontal field direction

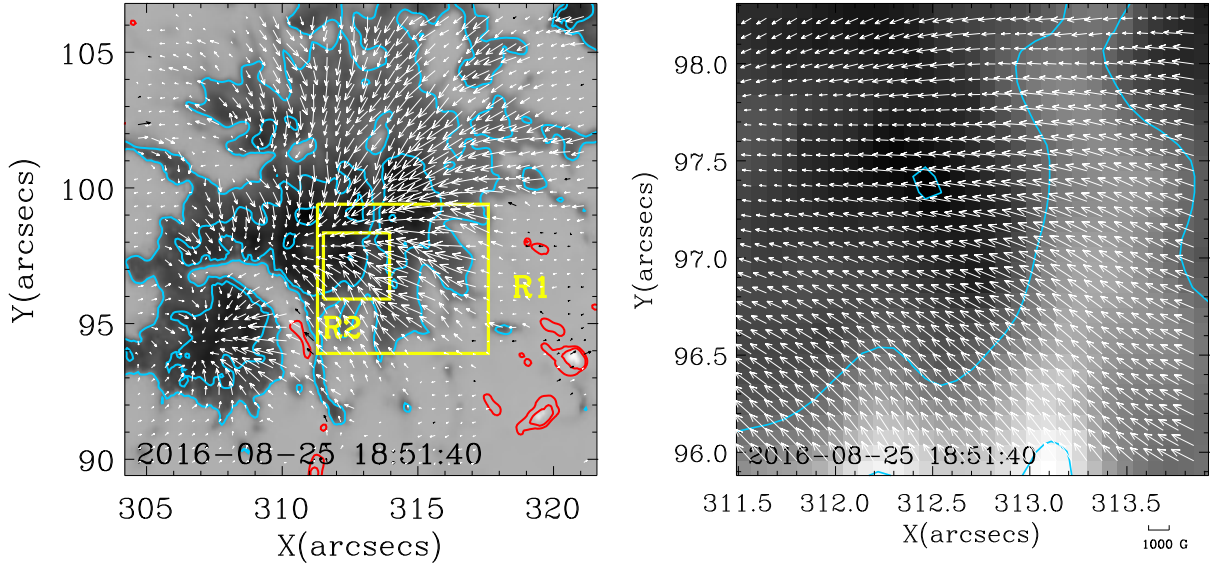


Fig. 5. Vector magnetogram of the FOV and a zoom-in area of R1 obtained from GST/NIRIS after removing the 180° ambiguity in the transverse field. The blue and red contours indicate the magnetic field B_z at -2300G , -1700G , -900G , 50G , and 150G respectively. The vertical component of vector magnetic field B_z in grey scale is overlaid with arrows. The arrows indicate the strength and direction of the transverse magnetic field.

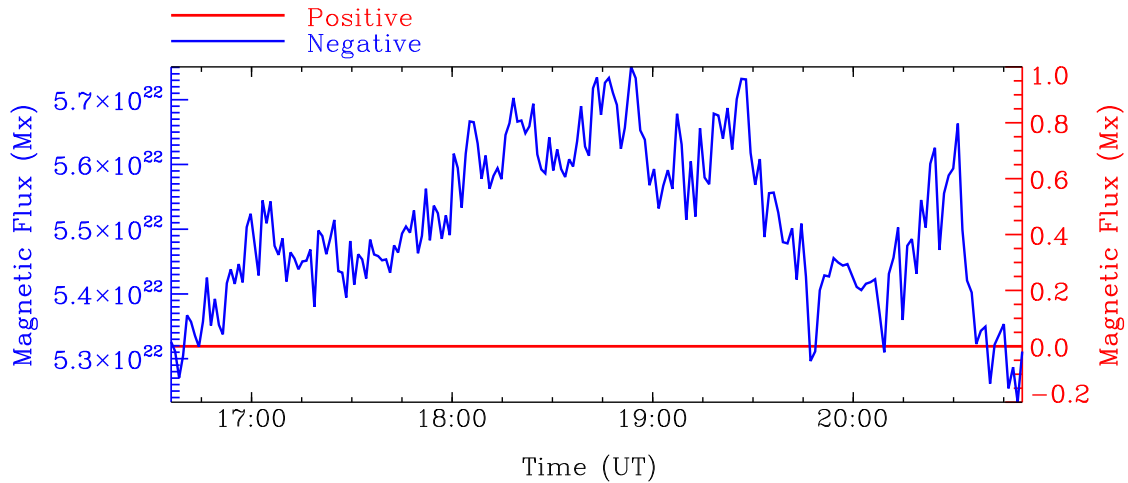


Fig. 6. Variation of both positive and negative magnetic flux in absolute values of the longitudinal magnetic field of R2 region marked in Fig. 5. During the jet eruption, some new flux emerges and magnetic reconnection may occur. The evolution of negative and positive flux are represented by blue and red color, respectively.

suggests a high gradient of connectivity at the footpoint of the fan-shaped jet.

This change in the horizontal magnetic field direction is kept as we go further away from the fan-shaped jet footpoint toward the west (see the right side of the R1 box). This change in orientation in the field is consistent with the diverging shape of the dark structures forming the fan-shaped jet observed in the $H_\alpha -0.8 \text{ \AA}$.

2.6. Brightenings at the jet front

In the course of the fan-shaped jet event (Sect. 2.2), we also identified EUV brightenings observed in the AIA channels. The left column of Fig. 7 shows the AIA images at 171 \AA for three instances. The red circle and the pink dots show respectively the location of the fan-shaped jet bright footpoint (Sect. 2.4) and the front of the fan shaped-jet in the H_α blue wing (Sect. 2.2). While no 171 \AA brightening is associated with the fan-shaped

jet footpoint, there are 171 \AA brightenings located at the front of the fan-shaped jet. Over the time interval of the fan-shaped jet, these EUV brightenings have a motion that is similar to the one of the fan-shaped jet along the south-east and north-west axes (Sect. 2.2).

These brightenings at the front of the fan-shaped jet are observed in all AIA channels except at 304 \AA . This can be explained by the fact that the 304 \AA filter is dominated by the emission of the He II line at 303.78 \AA , which is an optically thick line formed at chromospheric and transition region temperatures. Therefore, the filament and surge commonly appear dark in this filter. In the other channels, we observed a few bright pixels in the front of the jet. Due to the low resolution of AIA compared with the high resolution of the GST, these brightenings do not show any fine structure. They appear blurry in the images because the pixel size of AIA is large compared to the GST pixel size and, certainly, the intensity peaks only in a small area, as compared to the AIA pixel area. However, in the [movie](#),

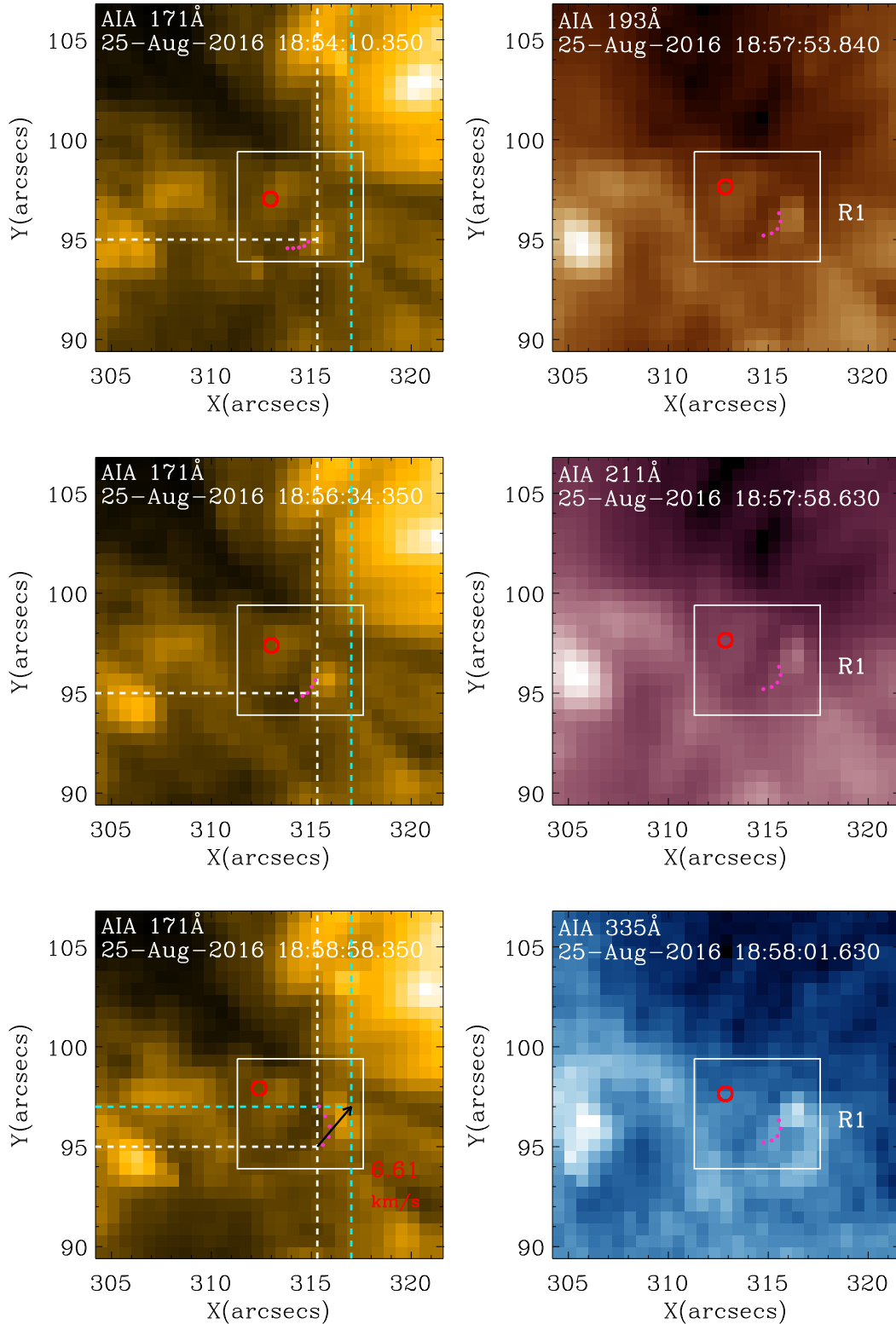


Fig. 7. Corona response observed with the different filters of SDO/AIA. R1 represents the area where the jet occurred. The footpoint and front of the jet are marked by red circle and magenta dots, respectively, as in Fig. 1. The brightening displacement and speed are marked on the bottom left corner panel with an arrow and a value of 6.61 km s^{-1} .

we can see that they are moving versus time around the front as the fan develops. Behind the front, dark absorption features correspond to the cool jet. The brightening is relatively obvious in 131 \AA , 171 \AA , 193 \AA , indicating that the jet front contains hot material, up to 10^5 or even 10^6 K . The brightenings in the front

of the jets may also correspond to enhancement of density due to compression in the corona.

We estimate the speed of the EUV brightening at 171 \AA . In Fig. 7 (left column), the white and light blue dashed lines shows respectively the initial and final location of the EUV

brightening. Assuming a uniform speed between those two times, we obtain a brightening velocity of approximately 6.61 km s^{-1} . This velocity is of the same order of magnitude as the speed of the fan-shaped jet (Sect. 2.2).

3. Discussion and conclusions

In this paper, we report on coordinated observations with the GST at BBSO and SDO/AIA of the active region NOAA 12579 on August 25, 2016. The observed event shows a fan-shaped jet occurring on the side of a light bridge (LB).

We obtained the following results:

1. The fan-shaped jet observed in absorption in the $H_\alpha \pm 0.8 \text{ \AA}$ shows a diverging shape. In the first phase, it exhibits a sweeping motion from the south to the north of the sunspot with an approximate velocity of $3.15\text{--}6.91 \text{ km s}^{-1}$ and in the second phase, the jet material is flowing back toward the photosphere. The computed Doppler diagram of the jet confirms these upflows and downflows (Sect. 2.2).
2. In the GST observations in TiO, we identified the LB close to the jet that divides the sunspot into two parts. However, the magnetic field analysis does not show any emergence of opposite polarity, as has been theoretically predicted for LBs (Sects. 2.4 and 2.5).
3. We also identified a bright point in the H_α blue wing located in the LB that is spatially consistent with the footpoint of the fan-shaped jet. This bright point is moving along the LB axis with an estimated speed of 2.1 km s^{-1} . By analyzing the H_α lines, we found that this bright point has the same spectral characteristic as Ellerman Bombs (Sect. 2.4). This suggests that this bright point may result from magnetic reconnection.
4. In analyzing the NIRIS vector magnetogram, we found that the magnetic field associated with the fan-shaped jet strongly diverges starting at the jet footpoint up to its front.
5. From the AIA observations, during the first phase of the jet, we observe a multi-thermal structure located at the front of the H_α jet and moving in time with it from south to north with an estimated speed of 6.6 km s^{-1} . This indicates that hot material up to 10^6 K is present at the fan-shaped jet front.

According to our analysis, we propose that the fan-shaped jet corresponds to the ejection of material along reconnecting magnetic field lines. The magnetic reconnection occurring in the photosphere-chromosphere is supported by the observation of EB's typical radiative signature at the bright jet's footpoint.

The diverging magnetic field supports the idea that the fan-shaped jet occurs in Quasi-separatrix layers (QSLs), which are topological elements connecting a bipolar field with a strong magnetic connectivity gradient, where thin and intense current sheet can be created (Demoulin et al. 1996). When 3D magnetic reconnection occurs in QSLs it creates an apparent slipping motion of the reconnecting field lines (Aulanier et al. 2006). Such a slipping motion of the field lines can be indirectly observed with the plasma filling the reconnecting field lines. In our event, the slipping reconnection may explain the shape and the dynamics of the fan-shaped jet observed in the H_α line.

Since the fan-shaped jet is anchored in the LB, an alternative scenario could be that the fan-shaped jet anchored in LB is a jet created by magnetic reconnection between the LB's emerging flux and the surrounding magnetic field of the sunspot. However, in our study, we did not identify in the NIRIS magnetogram opposite magnetic field emerging in the LB area (as we would have expected). We analyzed the HMI vector magnetograms during 24 hours before the event and no opposite polarity was detected – not even the LB was resolved. Nonetheless,

there is a factor of 6 (0.5 divided by 0.081 is equal to 6.17. The pixel size of HMI data before pre-processed is $0.''5$ and the pixel size of magnetic field data is $0.''081$) in the spatial resolution between GST/BBSO and HMI/SDO. It is likely that HMI/SDO is not equipped with the required resolution to detect emerging bipole and fast evolving LB.

Another interesting idea comes from theoretical models of sunspot formation in a magneto-convection environment (see Fig. 22 in Rempel 2012; Bharti et al. 2020). The sunspot, with its ephemeral LBs, is in a first phase of decay with intense fragmentation. The LBs are observed appearing and disappearing during the day. At the time of the jet, the LB is in a formation state with mainly bright points which are the footpoints of the jets. These bright points are brighter than the surrounding environment and, thus, hotter. They may rise by buoyancy from the subsurface. In theoretical models it is shown that magnetic field lines can be bent due to down-flows around convective cells (Bharti et al. 2020). Consequently it creates hair-pin shape magnetic field lines and opposite polarities may appear. The high spatial resolution of the GST could not be enough to resolve such bent magnetic field lines or the hair-pin turns in the subsurface of the Sun. We may wait for the new generation of ground-based telescopes such as DKIST and GIANT to resolve these fine structures.

It is worth mentioning that if magnetic reconnection occurs between some emerging bipoles and the strongly diverging field of the sunspot, magnetic reconnection across the QSLs can still take place and thus explain the shape and sweeping dynamics of the fan-shaped jet.

During the first phase, in addition to the H_α fan-shaped jet, a bright front is observed in most of the AIA wavelengths. Such a brightening indicates that the plasma in this region has been heated. Since it is located right at the front of the fan-shaped jet and it moves along with it at a speed that is on the same order of magnitude as the sweeping motion of the fan-shaped jet, we propose that the plasma may be heated by compression as the cold material propagates along the reconnecting field lines. The brightening disappears at the beginning of the second phase when the plasma is flowing back down toward the photosphere. We can speculate here that the jet material encounters a denser region that halt the propagation of the cold material that is then forced to flow back down.

Finally, we may also consider that the material inside the jets (considered as flux tubes) could be pushed up by increasing pressure due to MHD waves and convection. The absence of opposite polarities is in favor of this mechanism (Hollweg et al. 1982; Dey et al. 2022). A shock would be created in the corona, effectively stopping the ejected material, as proposed by Iijima & Yokoyama (2015). This mechanism ought to be further investigated in the future with high-resolution observations.

Acknowledgements. Y. Liu and G.P. Ruan acknowledge the support by the NNSFC grant 12173022, U1831107, 11790303 and 11973031. We are grateful to Véronique Bommier for the discussion on HMI vector magnetograms, to Jin Chunlan, Chen Yajie, Hou Zhenyong for the data discussion and to Vasilis Archontis and Robert Cameron for the possible mechanisms of jet initiation during the “Whole-Sun workshop in Blaise Pascal Institute”. W. Cao acknowledges support from US NSF AST-2108235 and AGS-1821294 grants. BBSO operation is supported by NJIT and US NSF AGS-1821294 grant. GST operation is partly supported by the Korea Astronomy and Space Science Institute and the Seoul National University. We thank SDO/HMI, SDO/AIA teams for the free access to the data.

References

Asai, A., Ishii, T. T., & Kurokawa, H. 2001, *ApJ*, 555, L65

- Aulanier, G., Pariat, E., Démoulin, P., & DeVore, C. R. 2006, *Aol. Phys.*, **238**, 347
- Bai, X., Socas-Navarro, H., Nóbrega-Siverio, D., et al. 2019, *ApJ*, **870**, 90
- Bharti, L. 2015, *MNRAS*, **452**, L16
- Bharti, L., Rimmele, T., Jain, R., Jaaffrey, S. N. A., & Smartt, R. N. 2007, *MNRAS*, **376**, 1291
- Bharti, L., Sobha, B., Quintero Noda, C., Joshi, C., & Pandya, U. 2020, *MNRAS*, **493**, 3036
- Cao, W., Gorceix, N., Coulter, R., et al. 2010, *Astron. Nachr.*, **331**, 636
- Cao, W., Goode, P. R., Ahn, K., et al. 2012, in Second ATST-EAST Meeting: Magnetic Fields from the Photosphere to the Corona, eds. T. R. Rimmele, A. Tritschler, F. Wöger, et al., *ASP Conf. Ser.*, **463**, 291
- Chae, J., Qiu, J., Wang, H., & Goode, P. R. 1999, *ApJ*, **513**, L75
- Chen, P.-F., Fang, C., & Ding, M.-D. 2001, *Chin. J. Astron. Astrophys.*, **1**, 176
- Chen, Y., Tian, H., Peter, H., et al. 2019, *ApJ*, **875**, L30
- Cheung, M. C. M., De Pontieu, B., Tarbell, T. D., et al. 2015, *ApJ*, **801**, 83
- Démoulin, P., Mandrini, C. H., van Driel-Gesztelyi, L., et al. 1996, in Astronomical Society of the Pacific Conference Series, eds. R. D. Bentley, & J. T. Mariska, *ASP Conf. Series*, **111**, 49
- De Pontieu, B., Title, A. M., Lemen, J. R., et al. 2014, *Aol. Phys.*, **289**, 2733
- De Pontieu, B., Polito, V., Hansteen, V., et al. 2021, *Aol. Phys.*, **296**, 84
- Dey, S., Chatterjee, P., & Murthy, N., et al. 2022, *Nat. Phys.*, **18**, 595
- Ellerman, F. 1917, *ApJ*, **46**, 298
- Fang, C., Tang, Y. H., Xu, Z., Ding, M. D., & Chen, P. F. 2006, *ApJ*, **643**, 1325
- Franz, M., & Schlichenmaier, R. 2013, *A&A*, **550**, A97
- Goode, P. R., & Cao, W. 2012, in Ground-based and Airborne Telescopes IV, eds. L. M. Stepp, R. Gilmozzi, & H. J. Hall, *SPIE Conf. Ser.*, **8444**, 844403
- Grubecka, M., Schmieder, B., Berlicki, A., et al. 2016, *A&A*, **593**, A32
- Hashimoto, Y., Kitai, R., Ichimoto, K., et al. 2010, *PASJ*, **62**, 879
- Heyvaerts, J., Priest, E. R., & Rust, D. M. 1977, *ApJ*, **216**, 123
- Hollweg, J. V., Jackson, S., & Galloway, D. 1982, *Aol. Phys.*, **75**, 35
- Iijima, H., & Yokoyama, T. 2015, *ApJ*, **812**, L30
- Iijima, H., & Yokoyama, T. 2017, *ApJ*, **848**, 38
- Joshi, R., Chandra, R., Schmieder, B., et al. 2020, *A&A*, **639**, A22
- Joshi, R., Schmieder, B., Tei, A., et al. 2021, *A&A*, **645**, A80
- Katsukawa, Y., Berger, T. E., Ichimoto, K., et al. 2007, *Science*, **318**, 1594
- Landi Degl'Innocenti, E. 1992, in *Magnetic field measurements*, eds. F. Sanchez, M. Collados, & M. Vazquez, 71
- Leka, K. D. 1997, *ApJ*, **484**, 900
- Leka, K. D., Barnes, G., Crouch, A. D., et al. 2009, *Aol. Phys.*, **260**, 83
- Lemen, J. R., Title, A. M., Akin, D. J., et al. 2012, *Aol. Phys.*, **275**, 17
- Li, T., Hou, Y., Zhang, J., & Xiang, Y. 2020, *MNRAS*, **492**, 2510
- Lim, E.-K., Yang, H., Yurchyshyn, V., et al. 2020, *ApJ*, **904**, 84
- Liu, Z., Xu, J., Gu, B.-Z., et al. 2014, *Res. Astron. Astrophys.*, **14**, 705
- Louis, R. E., Bayanna, A. R., Mathew, S. K., & Venkatakrishnan, P. 2008, *Aol. Phys.*, **252**, 43
- Louis, R. E., Beck, C., & Ichimoto, K. 2014, *A&A*, **567**, A96
- Nishizuka, N., Shimizu, M., Nakamura, T., et al. 2008, *ApJ*, **683**, L83
- Pariat, E., Schmieder, B., Berlicki, A., et al. 2007, *A&A*, **473**, 279
- Pesnell, W. D., Thompson, B. J., & Chamberlin, P. C. 2012, *Aol. Phys.*, **275**, 3
- Peter, H., Tian, H., Curdt, W., et al. 2014, *Science*, **346**, 1255726
- Raouafi, N. E., Patsourakos, S., Pariat, E., et al. 2016, *Space Sci. Rev.*, **201**, 1
- Rempel, M. 2012, *ApJ*, **750**, 62
- Rezaei, R., & Beck, C. 2015, *A&A*, **582**, A104
- Robustini, C., Leenaarts, J., de la Cruz Rodríguez, J., & Rouppe van der Voort, L. 2016, *A&A*, **590**, A57
- Robustini, C., Leenaarts, J., & de la Cruz Rodríguez, J. 2018, *A&A*, **609**, A14
- Rouppe van der Voort, L. H. M., Rutten, R. J., & Vissers, G. J. M. 2016, *A&A*, **592**, A100
- Roy, J. R. 1973, *Aol. Phys.*, **32**, 139
- Ruan, G., Schmieder, B., Masson, S., et al. 2019, *ApJ*, **883**, 52
- Samanta, T., Tian, H., Yurchyshyn, V., et al. 2019, *Science*, **366**, 890
- Scharmer, G., & Lofdahl, M. 1991, *Adv. Space Res.*, **11**, 129
- Schmieder, B., Joshi, R., & Chandra, R. 2021, *Adv. Space Res.*, **70**, 1580
- Schou, J., Scherrer, P. H., Bush, R. I., et al. 2012, *Aol. Phys.*, **275**, 229
- Shen, Y. 2021, *Proc. R. Soc. London Ser. A*, **477**, 217
- Shibata, K. 1982, *Aol. Phys.*, **81**, 9
- Shibata, K., Nakamura, T., Matsumoto, T., et al. 2007, *Science*, **318**, 1591
- Shimizu, T., Katsukawa, Y., Kubo, M., et al. 2009, *ApJ*, **696**, L66
- Su, J. T., Ji, K. F., Banerjee, D., et al. 2016, *ApJ*, **816**, 30
- Takasao, S., Isobe, H., & Shibata, K. 2013, *PASJ*, **65**, 62
- Tian, H., DeLuca, E. E., Cranmer, S. R., et al. 2014, *Science*, **346**, 1255711
- Tian, H., Yurchyshyn, V., Peter, H., et al. 2018, *ApJ*, **854**, 92
- Toriumi, S., Cheung, M. C. M., & Katsukawa, Y. 2015a, *ApJ*, **811**, 138
- Toriumi, S., Katsukawa, Y., & Cheung, M. C. M. 2015b, *ApJ*, **811**, 137
- Tsuneta, S., Ichimoto, K., Katsukawa, Y., et al. 2008, *Aol. Phys.*, **249**, 167
- Watanabe, H., Vissers, G., Kitai, R., Rouppe van der Voort, L., & Rutten, R. J. 2011, *ApJ*, **736**, 71
- Wöger, F., von der Lühe, O., & Reardon, K. 2008, *A&A*, **488**, 375
- Yang, H., Lim, E.-K., Iijima, H., et al. 2019a, *ApJ*, **882**, 175
- Yang, X., Yurchyshyn, V., Ahn, K., Penn, M., & Cao, W. 2019b, *ApJ*, **886**, 64
- Yuan, D., & Walsh, R. W. 2016, *A&A*, **594**, A101